

ISSN: (Print) (Online) Journal homepage: <https://www.tandfonline.com/loi/tbsd20>

Identification of novel dual acting ligands targeting the adenosine A2A and serotonin 5-HT1A receptors

Iman Touati, Mohnad Abdalla, Yassir Boulaamane, Nawal Al-Hoshani, Abdulaziz Alouffi, Mohammed Reda Britel & Amal Maurady

To cite this article: Iman Touati, Mohnad Abdalla, Yassir Boulaamane, Nawal Al-Hoshani, Abdulaziz Alouffi, Mohammed Reda Britel & Amal Maurady (18 Oct 2023): Identification of novel dual acting ligands targeting the adenosine A2A and serotonin 5-HT1A receptors, Journal of Biomolecular Structure and Dynamics, DOI: [10.1080/07391102.2023.2270753](https://doi.org/10.1080/07391102.2023.2270753)

To link to this article: <https://doi.org/10.1080/07391102.2023.2270753>



View supplementary material [↗](#)



Published online: 18 Oct 2023.



Submit your article to this journal [↗](#)




View related articles [↗](#)



View Crossmark data [↗](#)



Identification of novel dual acting ligands targeting the adenosine A2A and serotonin 5-HT1A receptors

Iman Touati^a, Mohnad Abdalla^b, Yassir Boulaamane^a, Nawal Al-Hoshani^c, Abdulaziz Alouffi^d, Mohammed Reda Britel^a and Amal Maurady^{a,e} 

^aLaboratory of Innovative Technologies, National School of Applied Sciences of Tangier, Abdelmalek Essaadi University, Tetouan, Morocco; ^bPediatric Research Institute, Children's Hospital Affiliated to Shandong University, Jinan, Shandong, China; ^cDepartment of Biology, College of Science, Princess Nourah bint Abdulrahman University, Riyadh, Saudi Arabia; ^dKing Abdulaziz City for Science and Technology, Riyadh, Saudi Arabia; ^eFaculty of Sciences and Techniques of Tangier, Abdelmalek Essaadi University, Tetouan, Morocco

Communicated by Ramaswamy H. Sarma

ABSTRACT

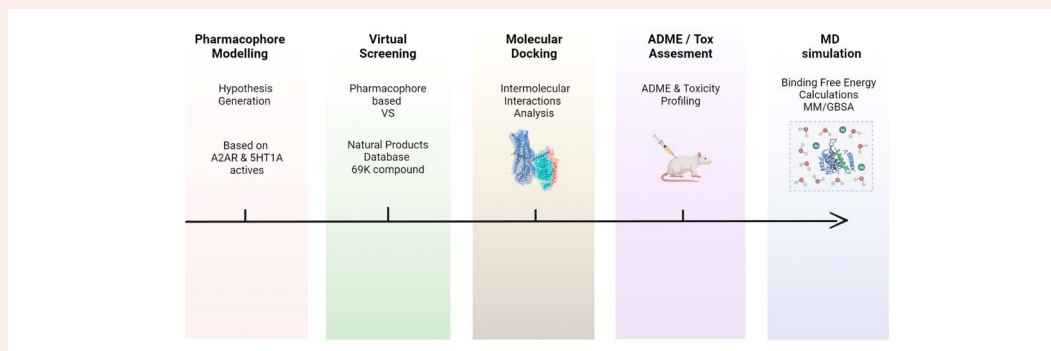
GPCRs are a family of transmembrane receptors that are profoundly linked to various neurological disorders, among which is Parkinson's disease (PD). PD is the second most ubiquitous neurological disorder after Alzheimer's disease, characterized by the depletion of dopamine in the central nervous system due to the impairment of dopaminergic neurons, leading to involuntary movements or dyskinesia. The current standard of care for PD is Levodopa, a dopamine precursor, yet the chronic use of this agent can exacerbate motor symptoms. Recent studies have investigated the effects of combining A2AR antagonist and 5-HT1A agonist on dyskinesia and motor complications in animal models of PD. It has been proved that the drug combination has significantly improved involuntary movements while maintaining motor activity, highlighting as a result new lines of therapy for PD treatments, through the regulation of both receptors. Using a combination of ligand-based pharmacophore modelling, virtual screening, and molecular dynamics simulation, this study intends on identifying potential dual-target compounds from IBScreen. Results showed that the selected models displayed good enrichment metrics with a near perfect receiver operator characteristic (ROC) and Area under the accumulation curve (AUAC) values, signifying that the models are both specific and sensitive. Molecular docking and ADMET analysis revealed that STOCK2N-00171 could be potentially active against A2AR and 5-HT1A. Post-MD analysis confirmed that the ligand exhibits a stable behavior throughout the simulation while maintaining crucial interactions. These results imply that STOCK2N-00171 can serve as a blueprint for the design of novel and effective dual-acting ligands targeting A2AR and 5-HT1A.

ARTICLE HISTORY

Received 5 June 2023
Accepted 7 October 2023

KEYWORDS




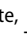


Ligand-based pharmacophore modelling; dual-target; molecular docking; ADMET; MD simulation; Parkinson's disease




1. Introduction

G-protein coupled receptors (GPCR) are the largest family of transmembrane proteins in humans, with ~800 members, half of which are olfactory receptors (Azam et al., 2020; Mori et al., 2022). The receptors possess seven membrane-

spanning domains linked by three intracellular and three extracellular loops (Lütjens & Rocher, 2017). They regulate a diverse array of physiological processes, making them prime drug targets (Hilger et al., 2018). More than half of non-

CONTACT Iman Touati  iman.touati@etu.uae.ac.ma  Laboratory of Innovative Technologies, National School of Applied Sciences of Tangier, Abdelmalek Essaadi University, Tetouan, Morocco; Mohnad Abdalla  mohnadabdalla200@gmail.com  Pediatric Research Institute, Children's Hospital Affiliated to Shandong University, Jinan, Shandong, 250022, China; Amal Maurady  amaurady@uae.ac.ma  Laboratory of Innovative Technologies, National School of Applied Sciences of Tangier, Abdelmalek Essaadi University, Tetouan, Morocco

 Supplemental data for this article can be accessed online at <https://doi.org/10.1080/07391102.2023.2270753>

© 2023 Informa UK Limited, trading as Taylor & Francis Group

olfactory receptors show a localized expression in the cerebral cortex (Hauser et al., 2017). Given their roles in regulating complex brain functions, it has been postulated that GPCRs make an attractive target for neurodegenerative disorders, including Parkinson's disease (PD) (Rahman et al., 2022). PD is a chronic neurological disorder that targets the geriatric population; two of its distinguishing hallmarks are the depletion of dopamine in the central nervous system (CNS) and the degeneration of dopaminergic neurons (Rascol et al., 2005).

The illness manifests itself in a wide spectrum of symptoms that affects patients to varying degrees; physical symptoms can range from limb stiffness to tremor and slowness of movements (Sveinbjornsdottir, 2016). Numerous palliative treatments are available for patients, some of which compensate for the lack of dopamine in the CNS, including L-DOPA, dopamine agonists, catechol-O-methyl transferase (COMT) inhibitors, and monoamine oxidase B (MAO-B) inhibitors (Cotzias et al., 1969; Tolosa et al., 1998). Others act on non-dopaminergic targets such as N-methyl-d-aspartate (NMDA) receptors, acetylcholinesterase (AChE), and adenosine A2A receptors (A2AR) (Cenci et al., 2022; Xu et al., 2005).

The adenosine A2A receptor, one of the three subtypes of adenosine receptors, is a member of class A GPCRs that can be found in various tissues throughout the body. Although its distribution predominates in specific regions of the brain where dopamine is highly concentrated, its expression can be traced, to a lesser extent, in other organisms such as the heart, lungs, spleen, blood platelets, and leukocytes (Glass et al., 1996; Jarvis et al., 1989).

A2ARs are highly expressed in GABAergic neurons, where they are co-localized with dopamine D2 receptors (Schiffmann et al., 2007). This unique localization suggests that A2ARs are involved in modulating motility (Mori, 2020). The link between A2AR and neurodegenerative illnesses is strong, albeit of complex nature. A2ARs are known to decrease the affinity of dopamine D2 receptors, stimulate the release of acetylcholine, and counteract the actions of dopamine, a key neurotransmitter to motor control (Chen & Cunha, 2020). Therefore, the blockade of A2AR through the administration of its antagonists could mitigate PD's symptoms and aid in regaining motor control (Cieślak et al., 2008).

5-hydroxytryptamine 1A (5-HT1A) receptor, another member of class A GPCRs, is one of the 14 subtypes of serotonin receptors that exhibit high expression in the limbic regions, lateral septum and raphe nuclei (Ohno et al., 2015). 5-HT1A receptors are associated with cognitive function and memory, whereby any dysfunction in 5HT1A receptors could lead to cognitive impairment (Azam et al., 2020; King et al., 2008). It has been shown that the activation of 5-HT1A by agonists or partial agonists alleviates motor symptoms in animal models of PD and MPTP-treated primates (Dupre et al., 2008). Other studies have revealed that the administration of different 5-HT1A agonists has anti-dyskinetic effects on patients with PD (Politis et al., 2014). Various preclinical and clinical studies have shown that selective 5-HT1A agonists can suppress motor complications induced by L-DOPA, suggesting their utility as a promising non-dopaminergic treatment for

PD therapy (Ghiglieri et al., 2016). Recent studies have investigated the effect of combination therapy (A potent 5-HT1A agonist and an A2AR antagonist) on dyskinesia in rat and non-human primate PD models. It has been shown that the combination of drugs has significantly improved involuntary movements, while maintaining motor activity (Pinna et al., 2023), unveiling as a result new and promising lines of therapy for Parkinson's disease. Figure 1 is a highly simplified depiction of the adenosine A2A and serotonin 1A receptors.

On these bases, identifying novel dual-acting ligands that can act on both A2AR and 5-HT1A receptors may prove a better perspective for treating PD. By implementing *in silico* methods; i.e. pharmacophore modelling, virtual screening, molecular docking, ADMET, molecular dynamics simulation, and binding free energy calculations, this study intends to identify natural therapeutics targeting A2A and 5-HT1A receptors for the treatment of Parkinson's disease.

2. Materials and methods

2.1. Ligand-based pharmacophore modelling

Pharmacophore models were developed from multiple ligands; for each target, a set of 25 known actives were retrieved from GPCRdb (<https://gpcrdb.org/>) (Munk et al., 2016). The 2D structures of the selected actives for A2AR and 5-HT1A are depicted in Supplementary Material (Figures S1 and S2, respectively). SDF files of the active set were downloaded from PubChem (<https://pubchem.ncbi.nlm.nih.gov/>) and prepared using the Ligprep module of Schrödinger suite (Kim et al., 2019; LigPrep, 2021). Pharmacophore modelling was carried out using PHASE, wherein the prepped ligands were automatically aligned, and a common feature pharmacophore was generated (Dixon, Smondyrev, et al., 2006; Dixon, Smondyrev, Knoll, et al., 2006; Madhavi Sastry et al., 2013). Hypothesis setting was set to match 50% of actives, the preferred minimum number of features was set to five and the remaining parameters were left as default.

To validate the performance and robustness of the generated pharmacophores, 14 commercially available antagonists of A2AR and 13 agonists of 5-HT1A were sourced from ChEMBL database (<https://www.ebi.ac.uk/chembl/>) and incorporated into DUD-E web server (<https://dud.docking.org/>) to generate custom-made decoys. For every active, 50 decoys (inactive) were generated, leading to a set of 14 actives and 700 decoys for A2AR and a database of 13 actives and 650 decoys for 5-HT1A (Gaulton et al., 2012; Huang et al., 2006).

2.2. Pharmacophore-based virtual screening

The top-ranking models for A2AR and 5-HT1A were used for pharmacophore-based virtual screening. The IBS natural compound collection database (<https://www.ibscreen.com/natural-compounds>) was utilized to screen for potential dual-acting hits targeting A2AR and 5-HT1A. A database housing 69,075 natural compounds, was processed using Ligprep and

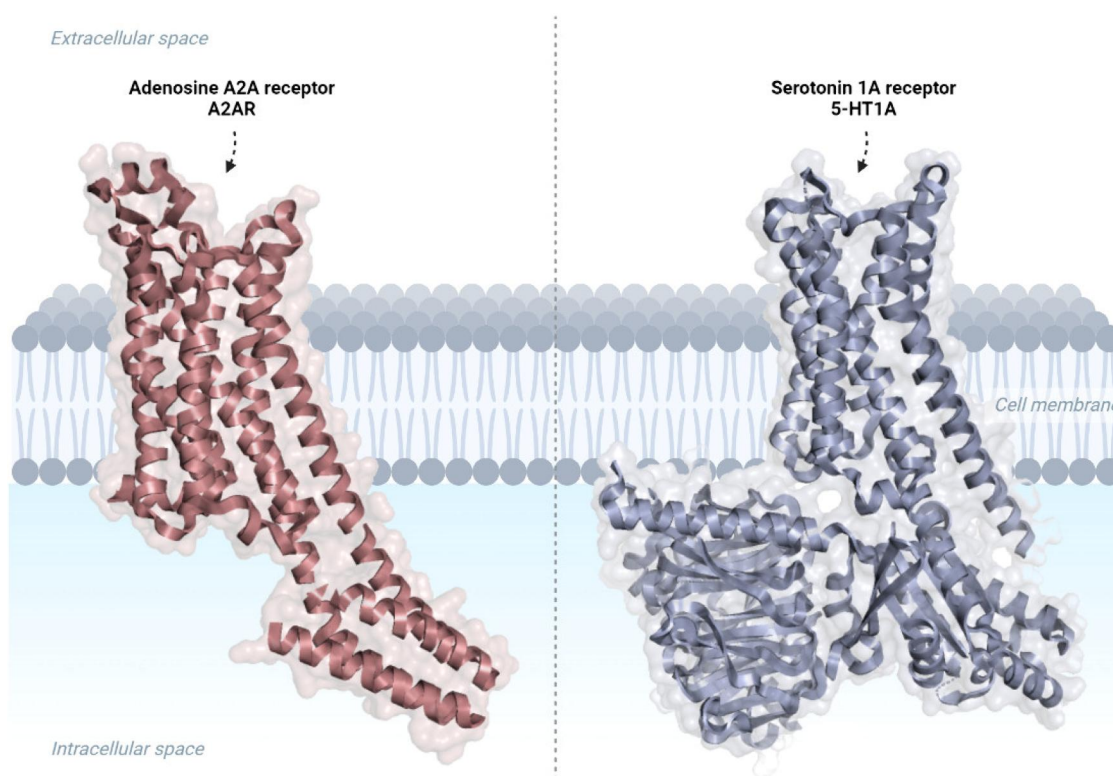


Figure 1. 3D representation of Adenosine A2A and serotonin 1A receptors.

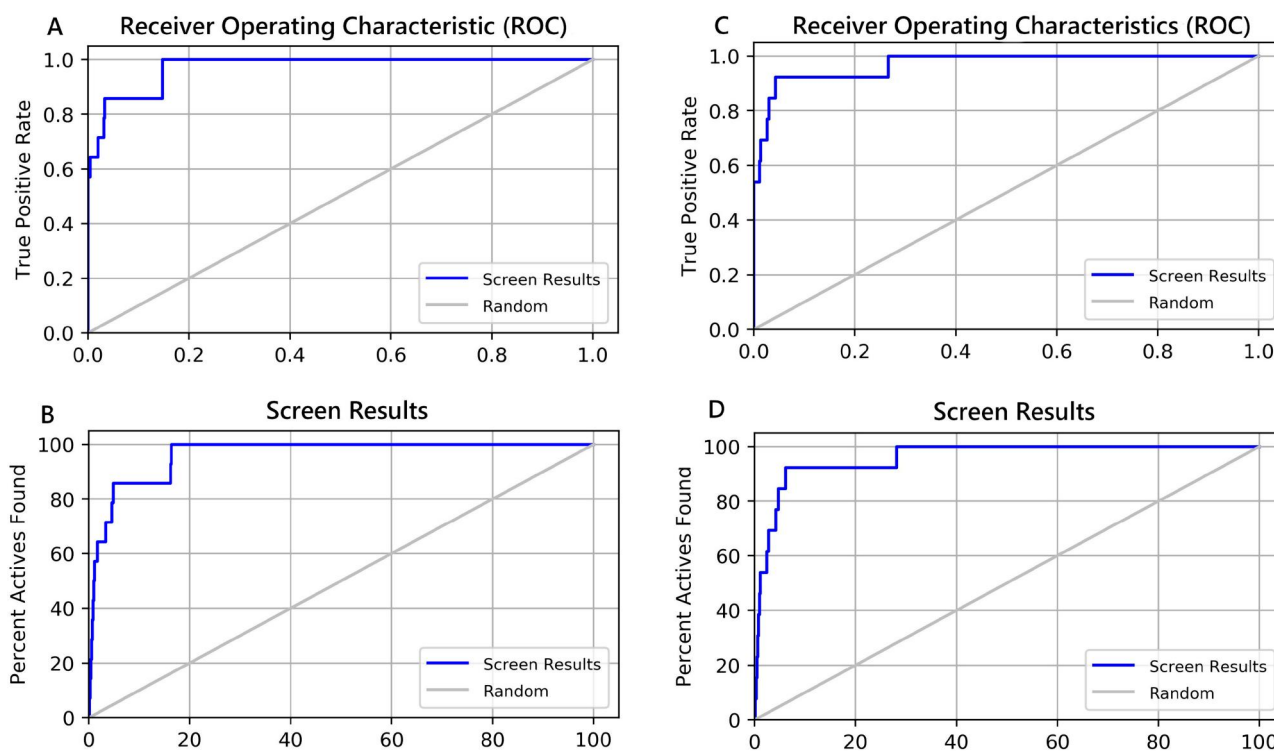


Figure 2. ROC plot (A,B) and percent screen plot (C,D) of ADRRR_2 and AHHR8-8, respectively.

shortlisted by applying Lipinski's filter in the Create Phase Database module of Schrödinger. An OPLS3 force field was used to minimize the compounds, while a minimum number of ligand conformers was set to 50. The database was subject to an initial screening using the A2AR pharmacophore

model; compounds bearing pharmacophore features of A2AR model were screened for a second time using the 5-HT1A pharmacophore. Compounds that were identified are endowed with features of both A2AR and 5-HT1A pharmacophore models.

2.3. Target preparation

The 3D crystal structure of the Adenosine A2A receptor complexed with antagonist ZM-241385 and Serotonin 1A receptor bound to agonist Aripiprazole (PDB ID: 5IU4 and 7E2Z, respectively) were retrieved from RCS Protein Data Bank (<https://www.rcsb.org/>) (Berman et al., 2003). Using the protein preparation wizard of Maestro, hydrogen atoms were added, bond orders were assigned and water molecules beyond 5 Å of the binding site were removed. Structures were minimized using the OPLS3 force field, while the binding pockets were identified by centering the grid box on the co-crystallized ligands (Madhavi Sastry et al., 2013; Schrödinger, LLC, 2021a).

2.4. Molecular docking

Molecules resulting from the pharmacophore searches were docked against A2AR and 5-HT1A binding pockets using the Glide Extra Precision docking protocol (XP) (Friesner et al., 2004, 2006). The top 10% of hits acquired from A2AR and 5-HT1A XP docking were overlapped to select common actives for both proteins.

2.5. ADME and toxicity assessment

Drug-likeness and ADME parameters were predicted using Qikprop of the Schrödinger suite (Schrödinger, LLC, 2021b), while the toxicity profile was assessed using ADMET Lab 2.0 web-server (<https://admetmesh.scbdd.com/>) (Xiong et al., 2021).

2.6. Molecular dynamics study

The protein-ligand complexes were ranked based on their intermolecular interactions with the targets and visual examination of their binding profiles. The top-ranked complexes were then chosen for MD simulation using Schrödinger's Desmond Module (Bowers et al., 2006; Schrödinger, LLC, 2021c).

The proteins were preprocessed and optimized using OPLS3e force field. The system was solvated in an orthorhombic box with periodic boundary conditions by adding TIP3P water molecules. The box was minimized, and the system was neutralized by adding Na⁺ and Cl⁻ (Abdalla et al., 2021, 2022). The simulation was carried out for 100 ns at a temperature of 310 K and a pressure of 1.013 bar. The MD simulation trajectory was analyzed using the simulation interaction diagram tool.

2.7. Binding energy calculation

The Prime Molecular Mechanics/Generalized Born Surface Area (MM/GBSA) was used to compute the binding free energy for the selected protein-ligand complexes (Jacobson et al., 2002, 2004; Schrödinger, LLC, 2021d), and was calculated using the following equation:

$$G(\text{bind}) = G_{\text{complex}} - G_{\text{protein}} - G_{\text{ligand}}$$

Where G_{complex} is the energy of the protein-ligand complex, G_{protein} is the energy of the protein and G_{ligand}

energy of the ligand (Abdalla & Rabie, 2023; Eltayb, Abdalla, et al., 2023; Eltayb, Abdalla, El-Arabey, et al., 2023).

3. Results and discussion

3.1. Pharmacophore model validation

The training set for each receptor generated 18 pharmacophore hypotheses for A2AR, and 40 models for 5-HT1A. The best 10 hypothesis models, ranked based on Phase Hypo Score, EF1%, BEDROC ($\alpha = 160.9$), ROC, AUC, and the number of retrieved actives are summarized in Tables 1 and 2, respectively. Six chemical features are provided by PHASE using the default settings: hydrogen bond acceptor (A), hydrogen bond donor (D), hydrophobic group (H), aromatic ring (R), negatively charged group (N), and positively charged group (P).

To validate the constructed models, four enrichment metrics were taken into consideration including Enrichment Factor 1% (EF1%), which stands for the fraction of retrieved actives after 1% of decoys have been screened, Area under the accumulation curve (AUAC), and receiver operating characteristic (ROC) both are indicative of the robustness and performance of the pharmacophore models. Values range from 0 to 1, 1 being the ideal case where all actives are retrieved, while 0 is a sign that the models cannot distinguish between actives and decoys (Giordano et al., 2022; Kumar et al., 2022). While the Boltzmann-enhanced discrimination of receiver operation characteristic (BEDROC), is a performance metric that can be interpreted as the probability of an active compound being ranked better than a compound selected at random while taking into account early recognition of true hits. As for AUAC and ROC, BEDROC ranges from 0 to 1.

Tables 1 and 2 report enrichment calculation results for A2AR and 5-HT1A, respectively.

It is noteworthy to point out that out of the 18 generated A2AR pharmacophore models, 10 had four features (AADR_1, AAAR_1, AADR_2, DRRR_1, ADRR_2, ADRR_1, ADRR_3, ADRR_4, AARR_1, AARR_2) while 8 models had five features (ADRRR_2, AADRR_1, AADRR_3, AAADR_1, AADRR_2, ADRRR_1, AADHR_1, AAADR).

The top 10 models displayed good enrichment metrics, with five hypotheses having an EF1% of 51 and a BEDROC ≥ 0.89 , two of which (ADRRR_1 and ADRRR_2) showed similar features. Upon investigating the ROC plots of the five first models, it seemed that ADRRR_2 had the steepest curve that plateaued out, as illustrated in Figure 2(A), which signifies that the model ranked active compounds higher than inactive ones (Moussa et al., 2021). ADRRR_2 was also able to recover all actives from the screened database. Taken together, it seems that the five-point pharmacophore ADRRR_2, is the best-performing model based on its overall enrichment metrics, with an EF1% of 51, BEDROC score of 0.89, an almost perfect ROC and AUAC (0.97 and 0.96, respectively), and was selected for further studies.

As for 5-HT1A, a total of 40 models were generated, 10 models having seven features, 10 with six features, 10 with five features, and 10 4-point models. Table 2 depicts the top

Table 1. Validation of the top 10 A2AR pharmacophore models.

| Hypothesis | Phase Hypo Score | EF1% | BEDROC 160.9 | ROC | AUAC | Total actives | Ranked actives | Matches |
|----------------|------------------|--------------|--------------|-------------|-------------|---------------|----------------|---------------|
| DRRR_1 | 1.17 | 51.00 | 0.97 | 0.86 | 0.92 | 14 | 12 | 4 of 4 |
| ADRR_4 | 1.17 | 51.00 | 0.93 | 0.86 | 0.91 | 14 | 12 | 4 of 4 |
| ADRRR_1 | 1.22 | 51.00 | 0.93 | 0.86 | 0.89 | 14 | 12 | 4 of 5 |
| ADRRR_2 | 1.18 | 51.00 | 0.89 | 0.97 | 0.96 | 14 | 14 | 4 of 5 |
| AADRR_3 | 1.23 | 51.00 | 0.88 | 0.93 | 0.92 | 14 | 14 | 4 of 5 |
| ADRR_1 | 1.20 | 43.71 | 0.87 | 0.86 | 0.92 | 14 | 12 | 4 of 4 |
| ADRR_2 | 1.14 | 36.43 | 0.80 | 0.85 | 0.92 | 14 | 12 | 4 of 4 |
| AAADR_1 | 1.09 | 29.14 | 0.56 | 0.92 | 0.91 | 14 | 14 | 4 of 5 |
| AADR_1 | 1.18 | 21.86 | 0.55 | 0.97 | 0.96 | 14 | 14 | 4 of 4 |
| AARR_1 | 1.09 | 21.86 | 0.54 | 0.84 | 0.89 | 14 | 12 | 4 of 4 |

EF1%: enrichment factor at 1% of the validation set; BEDROC 160.9: Boltzmann-enhanced discrimination of receiver operating characteristics; ROC: receiver operating characteristic curve value; AUAC: area under the accumulation curve.

Model in bold font is the best performing-model according to the enrichment metrics.

Table 2. Validation of the top 10 5-HT1A pharmacophore models.

| Hypothesis | Phase Hypo Score | EF1% | BEDROC 160.9 | ROC | AUAC | Total actives | Ranked actives | Matches |
|----------------|------------------|--------------|--------------|-------------|-------------|---------------|----------------|---------------|
| AAHHRR_1 | 1.37 | 47.54 | 0.89 | 0.90 | 0.90 | 13 | 12 | 4 of 6 |
| AHHRR_8 | 1.37 | 47.54 | 0.88 | 0.97 | 0.96 | 13 | 13 | 4 of 6 |
| AHHRR_4 | 1.34 | 47.54 | 0.91 | 0.89 | 0.91 | 13 | 12 | 4 of 5 |
| HHHRR_1 | 1.34 | 47.54 | 0.86 | 0.90 | 0.92 | 13 | 12 | 4 of 5 |
| AAHHHRR_2 | 1.41 | 39.62 | 0.72 | 0.96 | 0.95 | 13 | 13 | 4 of 7 |
| AAHHHRR_8 | 1.41 | 39.62 | 0.76 | 0.86 | 0.86 | 13 | 12 | 4 of 7 |
| AAHHHRR_7 | 1.41 | 39.62 | 0.66 | 0.81 | 0.80 | 13 | 12 | 4 of 7 |
| AHHHRR_2 | 1.38 | 39.62 | 0.81 | 0.87 | 0.87 | 13 | 12 | 4 of 6 |
| AHHRR_3 | 1.37 | 39.62 | 0.82 | 0.76 | 0.85 | 13 | 10 | 4 of 5 |
| AHHR_2 | 1.32 | 39.62 | 0.76 | 0.76 | 0.86 | 13 | 10 | 4 of 4 |

EF1%: enrichment factor at 1% of the validation set; BEDROC 160.9: Boltzmann-enhanced discrimination of receiver operating characteristics; ROC: receiver operating characteristic curve value; AUAC: area under the accumulation curve.

10 hypothesis ranked based on their overall enrichment metrics. Nine models (AAHHRR_1, AHHHRR_8, AHHRR_4, AAHHHRR_2, AAHHHRR_8, AAHHHRR_7, AHHHRR_2, AHHRR_3, AHHR_2) displayed the same 3 features: A (Hydrogen acceptor), H (Hydrophobic group) and R (Aromatic ring), while the last model had the least features, with three hydrophobic groups and two aromatic rings (HHHRR_1). The average EF 1% value for all 10 models was well over 42, while the highest value, 47.54, was observed in AAHHRR_1, AHHHRR_8, AHHRR_4, and HHHRR_1. All four models displayed good enrichment values, which indicates that the models are effective at distinguishing active molecules from inactive ones. AHHHRR_8 had the highest enrichment metrics, with an EF1% of 47.54, a BEDROC ($\alpha = 160.9$) value of 0.88, ROC of 0.97, and AUAC value of 0.96 and was selected for virtual screening.

ROC and percent screen plots for ADRRR_2 and AHHHRR_8 are portrayed in Figures 2(A–D), respectively. The ideal model has no overlap in two distributions, meaning that the ROC curve passes through the upper left corner and has perfect discrimination (100% specificity, 100% sensitivity).¹ As illustrated in Figure 2, all curves (in blue) are close to the upper left corner, which signifies that both models are sensitive and specific and can be used to map selective A2AR/5-HT1A ligands.

3.2. Pharmacophore-based virtual screening results

Virtual screening was conducted using the phase ligand-screening module of Schrödinger. The IBS database was screened using the selected A2AR model (ADRRR_2) using a 5 out of 5 restriction. Out of 69075 compounds, 1153 were identified to have the required pharmacophore features.

These hits were screened again using 5-HT1A model (AHHHRR-8). Initially, a query of six features was very restrictive and retrieved no hits, and the number of pharmacophore matches were reduced to five features. A hit list of 168 candidates were identified bearing features of both A2AR and 5-HT1A pharmacophore models. Figure 3 is a visual representation of the site type and pharmacophore features of ADRRR_2 and AHHHRR-8.

3.3. Validation of docking protocol

The docking protocol was validated by re-docking the native ligands back to their binding pockets and computing their RMSD. As depicted in Figure 4, results revealed that re-docking of ZM-241385 had an RMSD value of 0.0062, while re-docking of Aripiprazole showed an RMSD of 0.8674. All values fall within the 2.0 Å range, which indicates that the docking protocol was successful (Hadni & Elhallaouia, 2022).

3.4. Molecular docking results

The 168 hits retrieved *via* virtual screening were docked into the binding pocket of A2AR and 5-HT1A using extra precision mode (XP). The top 10% of hits for each target, ranked based on the computed docking score, were overlapped to identify potential dual ligands. Reference drugs were used as a baseline for comparing the interactions of potential hits. Table 3 summarizes the docking score and intermolecular interactions of the identified ligands, as well as the drugs of reference. The binding modes of the two identified hits are reported in Figure 5. Images were rendered using PyMOL visualization software.²

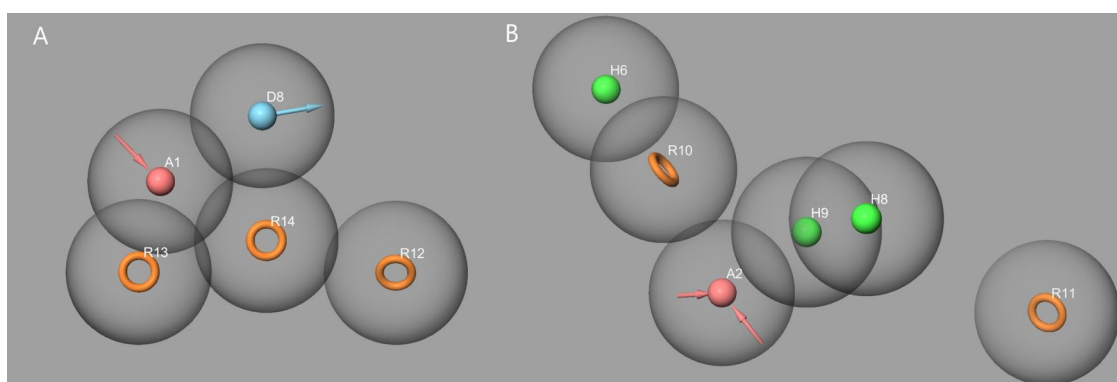


Figure 3. Pharmacophore features of (A) ADRRR_2 and (B) AHHR-8 models. The feature types are hydrogen bond acceptor (red), hydrogen bond donor (sky blue), aromatic ring (orange), and hydrophobic group (green).

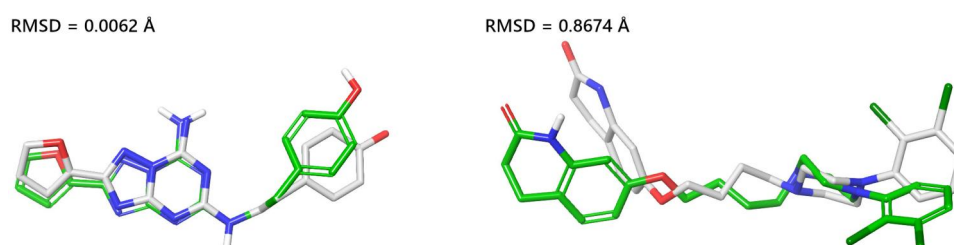


Figure 4. Superposition of native (in white) and re-docked (in green) ligands.

Table 3. Docking score and interacting residues of identified hits.

| ID | A2A | | | 5-HT1A | | |
|-------------------------------|--------------------------|--|--|--------------------------|---|--|
| | Docking score (Kcal/mol) | H-bonds | π - π interactions | Docking score (Kcal/mol) | H-bonds | π - π interactions |
| ZM-241385 | -10.8 | Asn-253 ^{6.55} Glu-169 ^{ECL2} | Phe-168 ^{ECL2} His-250 ^{6.52} | - | - | - |
| Aripiprazole STOCK2N-00171 | -11.7 | Ala-59 ^{2.56} Ile-66 ^{2.63} Phe-168 ^{ECL2} Asn-253 ^{6.55} | Phe-168 ^{ECL2} His-264 ^{6.66} | -5.3 -7.6 | Asp-116 ^{3.32} Cys-120 ^{3.36} Tyr-390 ^{7.42} | Phe-112 ^{3.28} Phe-361 ^{6.51} |
| STOCK2N-00446 | -11.1 | Asn-253 ^{6.55} Phe-168 ^{ECL2} Glu-169 ^{ECL2} | Phe-168 ^{ECL2} | -7.1 | Ile-189 ^{ECL2} | Tyr-96 ^{2.63} |

ZM-241385 is shown interacting with pivotal amino acid residues from the binding pocket of A2AR, the ligand was seen involved in H-bonding with polar residue Asn 253^{6.55} (numbering scheme according to Ballesteros and Weinstein 1995) and Glu 169^{ECL2}. Two additional hydrophobic interactions, involving Phe 168^{ECL2} of the second extracellular loop (ECL2) and the aromatic His 250^{6.52} located in the transmembrane domain, were also stabilizing the ligand inside the binding pocket. These results seem in congruent with the intermolecular interactions reported in the literature (Lebon et al., 2011). However, Aripiprazole did not seem to form any interactions within the active site of 5-HT1A, which would explain the low binding affinity (-5.39 Kcal/mol). It was previously shown that two types of interactions characterize the binding of high affinity agonists; a salt bridge interaction involving a highly conserved aspartate residue Asp 116^{3.32}, and an edge-to-face π - π interaction with aromatic residues from a hydrophobic pocket adjacent to Ser 199^{5.43} and Thr 200^{5.44} (Sukalovic et al., 2012).

STOCK2N-00171 is interacting, within 5-HT1A binding pocket, *via* the formation of H-bond with Cys 120^{3.36} and

aromatic amino acid Tyr 390^{7.42}. The lack of positively charged groups in STOCK2N-00171 has hindered the formation of salt bridge interactions with Asp 116^{3.32}, although the ligand sits in close proximity to the carboxylate group of the residue's side chain. While it has been established that this salt bridge is a crucial interaction stabilizing the complex, the ligand compensates for the lack of it by forming two strong hydrogen bonds with Asp 116^{3.32}; the amine group of imidazole moiety is interacting at a distance of 1.82 Å, while the hydroxyl group in phenol sits at a distance of 1.9 Å. The ligand also engages with the hydrophobic part of the binding site formed by Trp 358^{6.48}, Phe 361^{6.51} of the 6th transmembrane helix, and Phe 390^{7.42} *via* π - π interactions with Phe 361^{6.51}, and an additional hydrophobic interaction involving Phe 112^{3.28} and the 5-hydroxy-2-methyl pyran moiety. These aromatic-aromatic interactions have been previously reported to stabilize the ligand within the binding pocket (Zlatović et al., 2006).

Due to the bulky nature of STOCK2N-00446, the tricyclic part of the molecule sits at the surface of the binding pocket while the 5-methoxyindole section is embedded close to Ser

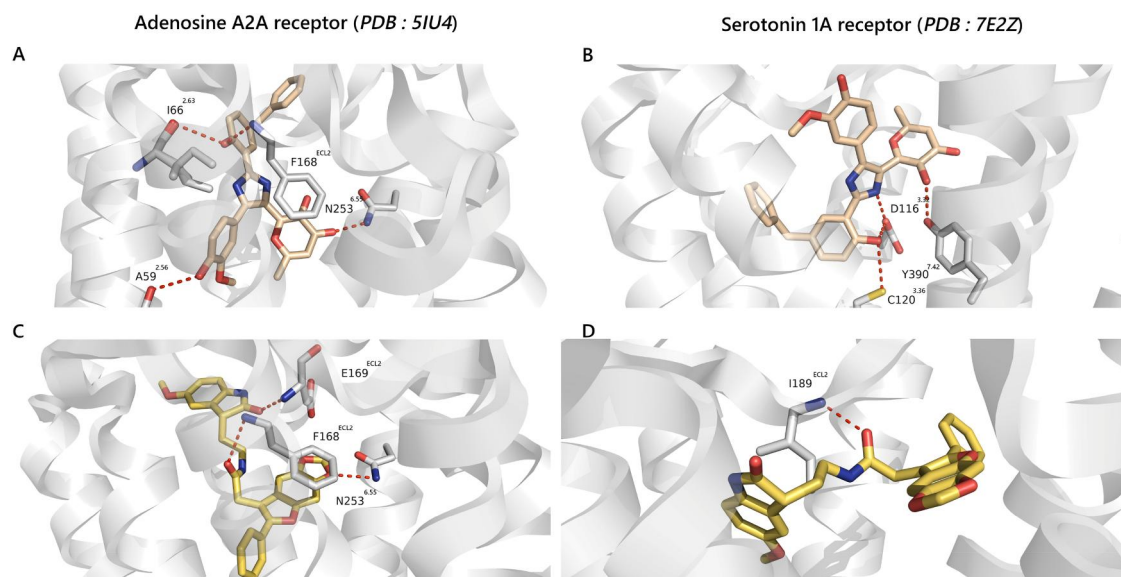


Figure 5. 3D views of molecular interactions of STOCK2N-00171 (A,B) STOCK2N-00446 (C,D) within the binding pocket of A2AR and 5-HT1A, respectively, numbering scheme according to Ballesteros and Weinstein.

199^{5.43} and Thr 200^{5.44}. The ligand is engaging in H-bond formation with Ile 189^{ECL2} of the extracellular loop and a single hydrophobic interaction involving Tyr 96^{2.63}. Since extracellular loops are known for their unstable nature, it seems that the H-bond involving Ile 189 of ECL2 does not contribute to stabilizing the complex (Zlatović et al., 2006), which might explain the difference in the binding score of STOCK2N-00171 and STOCK2N-00446 (−7.6 and −7.1 Kcal/mol, respectively).

STOCK2N-00171 has retained the same pivotal interactions observed with the binding of ZM-241385, the ligand is in contact with Asn 253^{6.55} through H-bond formation and is involved in π -stacking with the aromatic side chain of Phe 168^{ECL2} while interacting with the amine group of the α -carbon *via* a single hydrogen bond. Although the two interactions involving Glu 169^{ECL2} and His 250^{6.52} seen with the reference were lost, the binding score does not seem to be affected (−10.8 Kcal/mol for ZM-241385, −11.7 Kcal/mol for STOCK2N-00171). The difference in affinity could be accredited to the three additional interactions involving Ala 59^{2.56} and Ile 66^{2.63} of the second transmembrane helix, and the hydrophobic interaction with His 264^{6.66}. STOCK2N-00446 also mimics the interactive pattern of the reference, with three π - π interactions involving the aromatic ring of Phe 168^{ECL2} stabilizing the tricyclic portion of the ligand within the binding cavity and an H-bond with Asn 253^{6.55}. The two carbonyl groups pertaining to the ligand are in close contact with Glu 169^{ECL2} and Phe 168^{ECL2} and establish two additional hydrogen bonds. Both hits seem to interact with biologically relevant amino acid residues; previous mutagenesis studies have highlighted the crucial role of Asn 253^{6.55} and Phe 169^{ECL2} in ligand binding (Lane et al., 2012).

Results strongly indicate that STOCK2N-00171 exhibits a far more superior binding profile and establishes contact with crucial amino acid residues from both A2AR and 5-HT1A binding cavities. As a result, STOCK2N-00171 was selected for further analysis.

3.5. ADME/TOX analysis

Table 4 summarizes the results of the physicochemical evaluation generated by the Qikprop module. Seven descriptors were used to assess the drug-likeness of the selected hit, including, aqueous solubility (QPlogS), human serum albumin binding (QPlogKhsa), blood-brain barrier permeability (QPlogBB), and human intestinal absorption (HOA). Data revealed that the selected hit along with the two positive controls all fall within the recommended range for molecular weight, number of hydrogen bond donors, and number of hydrogen bond acceptors. The three molecules were also within the acceptable range for QPlogKhsa, exhibited high intestinal absorption, and could easily cross the blood–brain barrier. STOCK2N-00171 displayed low solubility, which could limit its oral bioavailability and dissolution, however, it should not be a determining factor to rule out the ligand as a drug candidate, especially since a good majority of commercially available drugs fall into this category (Liu et al., 2010).

Toxicity analysis, summarized in Table 5, has pointed out that the two reference drugs are flagged as hERG + blockers and display as a result high potential for cardio-toxicity. The controls also have a high potential to induce liver toxicity. ZM-241385 showed high toxicity and carcinogenic effect. However, it was shown that STOCK2N-00171 was safe on all levels, with values that did not exceed the standard range.

3.5. MD simulation analysis

3.5.1. Protein-ligand interaction contact analyses

MD simulation was carried out for the top scoring compound based on the docking score and key interactions, two complexes (STOCK2N-00171-A2AR and STOCK2N-00171-5-HT1A) along with the two references (ZM-241385-A2AR and Aripiprazole-5-HT1A) used as positive control were selected for further analysis.

Table 4. ADME properties of identified hits as predicted by Qikprop.

| Compound ID | M.W ^a | Donor HB ^b | Accept H.B ^c | QPlogS ^d | QPLogKhsa ^e | QPlogBB ^f | HOA ^g |
|---------------|------------------|-----------------------|-------------------------|---------------------|------------------------|----------------------|------------------|
| ZM-241385 | 337.340 | 4 | 6.750 | -4.023 | -0.204 | -1.891 | 73.446 |
| Aripiprazole | 448.391 | 1 | 6.250 | -6.359 | 0.864 | -0.066 | 100 |
| STOCK2N-00171 | 90.480 | 4 | 7 | -7.088 | 0.843 | -1.961 | 90.48 |

^aMolecular weight of the molecule (range: 130.0–725.0).

^bEstimated number of hydrogen bonds that would be donated by the solute to water molecules in an aqueous solution (range: 0.0–6.0).

^cEstimated number of hydrogen bonds that would be accepted by the solute from water molecules in an aqueous solution (range: 2.0–20.0).

^dPredicted aqueous solubility (range: -6.5–0.5).

^ePrediction of binding to human serum albumin (range: -1.5–1.5).

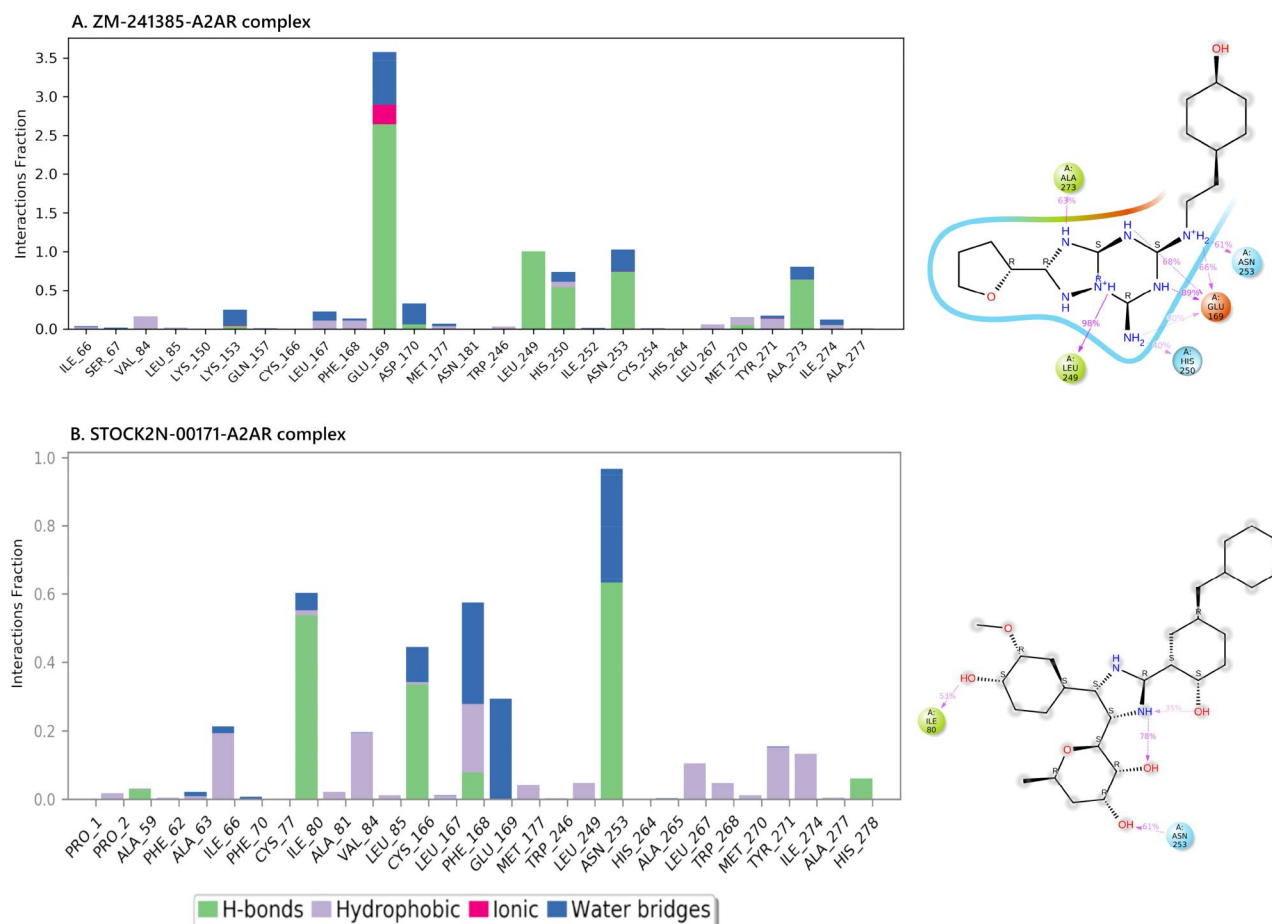
^fPredicted brain/blood partition coefficient (range: -3.0–1.2).

^gPredicted human oral absorption on 0–100% scale (>80% is high <25% is poor).

Table 5. Toxicity prediction as predicted by ADMET lab.

| Compound ID | hERG blockers | H-HT | Rat oral acute toxicity | FDAMDD | Carcinogenicity |
|---------------|---------------|-------|-------------------------|--------|-----------------|
| ZM-241385 | 0.805 | 0.995 | 0.547 | 0.923 | 0.944 |
| Aripiprazole | 0.996 | 0.824 | 0.972 | 0.546 | 0.363 |
| STOCK2N-00171 | 0.022 | 0.266 | 0.095 | 0.126 | 0.05 |

H-HT: human hepatotoxicity; FDAMDD: maximum recommended daily dose.

**Figure 6.** Protein-ligand interaction profile for A2AR in complex with (A) ZM-241385 and (B) STOCK2N-00171 and their 2D diagram of contact (right).

Figures 6 and 8 summarize the protein ligand interaction of STOCK2N-00171 complexed with A2AR and 5-HT_{1A}, respectively. Figure 6(A) reveals that ZM-241385 is in contact with Glu 169^{ECL2} through direct H-bonding and water-mediated hydrogen bonds with a normalized value of >3.5, meaning that these interactions were maintained for 350% of the simulation runtime. This indicates that Glu 169^{ECL2} is engaging in multiple interactions of a single type with the

reference. Other hydrophilic interactions can be spotted involving Leu 249^{6,51}, His 250^{6,52}, Asn 253^{6,55}, and Ala 273^{7,37}, with an occupancy of 98, 40, 61, and 63%, respectively. It seems that both H-bonding and water-mediated contacts were the two vital interactions stabilizing ZM-241385, with little to no importance for hydrophobic contacts and limited ionic interactions. However, STOCK2N-00171-A2AR complex had a different interaction profile.

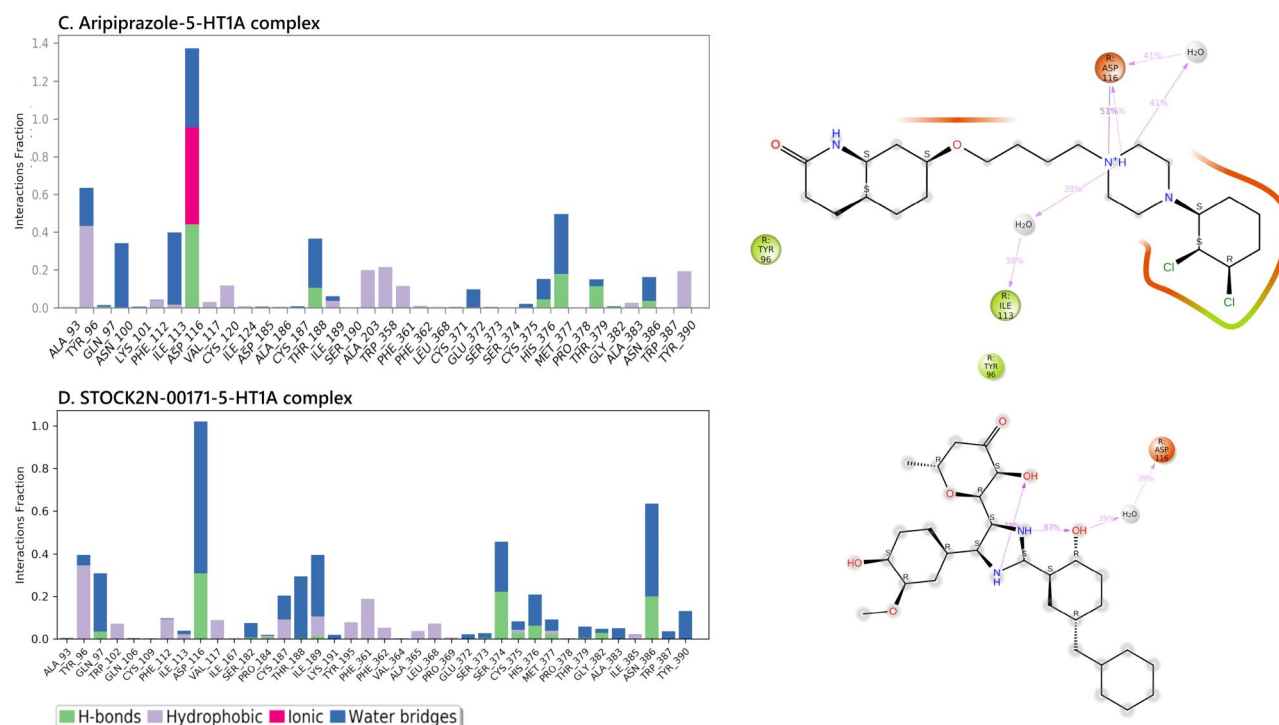


Figure 7. Protein-ligand interaction profile for 5-HT1A in complex with (A) Aripiprazole and (B) STOCK2N-00171.

As depicted in Figure 6(B), the ligand was bound to Ile 80^{3.28}, Cys 166^{ECL2}, and Asn 253^{6.55} via H-bonding with normalized values of 0.53, 0.33, and 0.61, respectively. Asn 253^{6.55} also interacted through water bridge contacts along with Phe 168^{ECL2} and Glu 169^{ECL2}, which were maintained effectively for 98, 58, and 29%, respectively, over the simulation runtime. Hydrophobic interactions mediated by Ile 66^{2.63}, Val 84^{3.32}, and Phe 168^{ECL2} were also observed to interact with an occupancy of ≤ 0.3 . Key interactions reported previously by the docking study were maintained throughout the 100 ns, which could indicate that the complex did not witness a drastic change in conformation and that STOCK2N-00171 is relatively stable inside the binding pocket of A2AR.

The interactions involving STOCK2N-00171 and Aripiprazole complexed with 5-HT1A were also monitored throughout the 100 ns simulation time, Figure 7 depicts the results.

It is noteworthy to mention that both complexes have virtually similar profiles except for the lack of an ionic bond involving Asp 116^{3.32} and STOCK2N-00171. Asp 116^{3.32} is in contact with Aripiprazole through a salt bridge interaction, which was maintained for 51% of the simulation time. Asp 116^{3.32} also formed direct and indirect (water bridge contact) H-bond interactions, with a high occupancy of ≥ 1.4 . The most prominent interactions seem to be water bridged interactions and hydrophobic contacts. Water mediated interactions involving Tyr 96^{2.63}, Asn 100^{2.67}, Ile 113^{3.29}, Thr 188^{ECL2}, and Met 377^{ECL3} persisted throughout the simulation with a frequency of ≥ 0.62 , 0.38, 0.4, 0.36, and 0.5, respectively.

Although STOCK2N-00171 lost a salt bridge interaction to Asp 116^{3.32}, a strong hydrophilic interaction can be seen involving the polar residue with a frequency $>100\%$, as illustrated in Figure 7(D). Additionally, Gln 97^{2.64}, Thr 188^{ECL2}, Ile

189^{ECL2}, Ser 374^{ECL3}, and Asn 384^{7.36} contributed to water mediated contacts. Asn 386^{7.38}, in particular, has been reported to be a crucial amino acid for the binding of selective 5-HT1A ligands (Kroeze et al., 2002) and is seen interacting with STOCK2N-00171 with an occupancy of 0.62. The ligand also forms hydrophilic interactions with Ser 374^{ECL3} from the third extracellular loop, for about 40% of the production runtime, which was not reported previously in the docking studies. These newly gained interactions might suggest that the ligand underwent large conformational changes to interact with these amino acids.

3.5.2. Complex deviation and fluctuation

Root-mean-square deviation plots, depicted in Figure 8, describe the structural deviations of a given protein with respect to the initial structure at each moment of the simulation.

According to the plots in Figure 8(A), it can be seen that the ZM-241385-A2AR complex is witnessing major fluctuations in the initial 50 ns of the simulation. The system then stabilizes with slight deviations recorded around 60 and 80 ns and peaks at ≈ 3.6 Å. The initial jump in RMSD could be due to the structural rearrangement of the second intracellular and extracellular loops and at the level of the fifth and sixth helices, which is in line with the findings of Novikov et al. (2013). Similarly, the STOCK2N-00171-A2AR complex, in Figure 8(B), reaches equilibrium after the 40 ns mark, ligand RMSD peaks at around 3.8 Å and levels out at 3.4 Å for the rest of the simulation. The C α -RMSD also exhibits similar stable behavior, averaging around ≈ 3.2 Å, with a slight hiccup at 60 ns. It is evident that STOCK2N-00171-A2AR complex is considerably stable throughout the simulation.

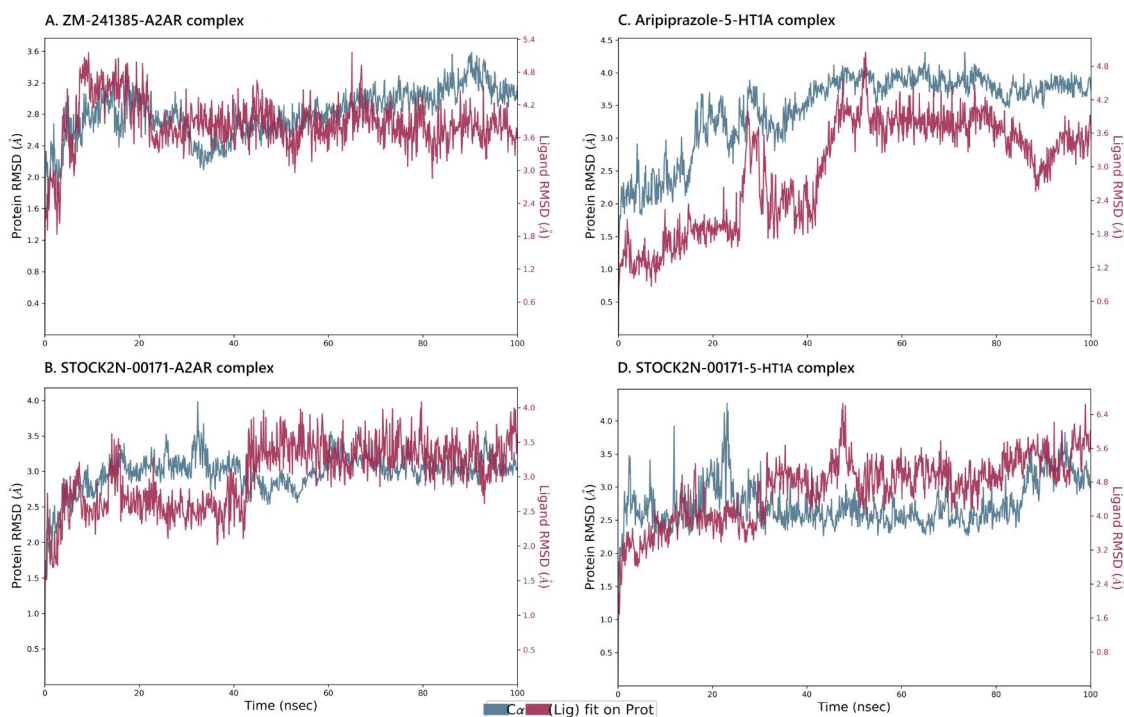


Figure 8. The root-mean-square deviations (RMSD) for backbone atoms and ligands.

As for the Aripiprazole-5-HT1A complex, the largest fluctuations are recorded in the first stages of the simulation; the protein RMSD increases progressively in the initial 50 ns of the simulation, only to reach a plateau at around 3.8 Å and stabilize for the rest of the production runtime. However, the ligand RMSD shows large fluctuations at 30 and 50 ns, which peaked at ≤ 4 and 5 Å, respectively. The complex reaches equilibrium in the small window of 50–80 ns, followed immediately by a drop to 2.6 Å. STOCK2N-00171 bound to 5-HT1A seems to exhibit fewer fluctuations relative to the positive control, the system converges after the initial 30 ns of the simulation, with a C α -RMSD lower than 3 Å while the ligand RMSD acquires equilibrium after 40 ns, averaging around 5 Å. This implies that the complex showed high stability across the simulation time.

The root-mean-square deviation (RMSF) graphs were also plotted to assess the effect of ligand binding on key amino acid residues. Results are illustrated in Figure 9.

Knowing the architecture of receptors from the GPCR family, the plots can be divided into several sections with distinct dynamical behaviors; intracellular and extracellular loops (ICLs and ECLs) which are inherently unstable, and transmembrane helices (TMs) which are expected to be the most stable regions. As illustrated in Figure 9(A), the region right before residue no. 50, right after residue 100 and right after residue 200 which coincide with the intracellular loop 1 (ICL1), intracellular loop 2 (ICL2), and intracellular loop 3 (ICL3), respectively, witness the highest fluctuations, despite the fact that they are not directly involved in the binding of ZM-241385. This points to the flexible and dynamic nature of loops, however, deviations witnessed in these regions are still under the acceptable range of 3 Å. The second extracellular loop (around residue 150) and the sixth helix (around residue 250) are also experiencing minor fluctuations in the

range of 2.4 Å. These regions correlate with key amino acids of A2AR (Phe 168^{ECL2}, Glu 169^{ECL2}, His 250^{6.52}, and Asn 253^{6.55}) involved in the binding of the drug of reference. This clearly indicates that the active site remains stable throughout the simulation.

Although ZM-241385 and STOCK2N-00171 have very similar RMSF profiles, it is evident that the binding of STOCK2N-00171 has prompted more fluctuations in ICL2, ECL2, and ICL3 compared to the drug of reference. A sharp increase of $\cong 1$, 1.8, and 1.5 Å in RMSF was recorded in each region, respectively. This could be due to the residues shifting in response to the binding of the ligand to better accommodate its bulky structure.

In the case of 5-HT1A, Figure 9(C) shows that regions with significantly increased RMSF values are captured near 150 and 250 with values exceeding the 3 Å threshold, these regions are located, respectively in the second and third extracellular loops which explains the increased mobility that can be seen in the plots. Significant fluctuations can be observed near residue 200, which roughly correlates to the sixth helix. By comparing the change in RMSF between the ligand-bound and Apo form (Figure S5, in Supplementary Material), it seems that the latter is also witnessing high fluctuations in these regions, particularly in the region right before residue 200 which peaked at 8.81 Å. Although this region does not seem to be involved in any interaction, the residue was significantly stabilized upon ligand binding.

The RMSF profile of STOCK2N-00171 was very reminiscent of the control, with the second and third extracellular loops experiencing major fluctuations, with values reaching up to 4.2 Å. It is possible to infer that the binding of STOCK2N-00171 also elicits a decrease in the region's flexibility before residue 200, with a drop of $\cong 3.9$ Å compared to the Apo form. It should also be noted that the crucial amino acids,

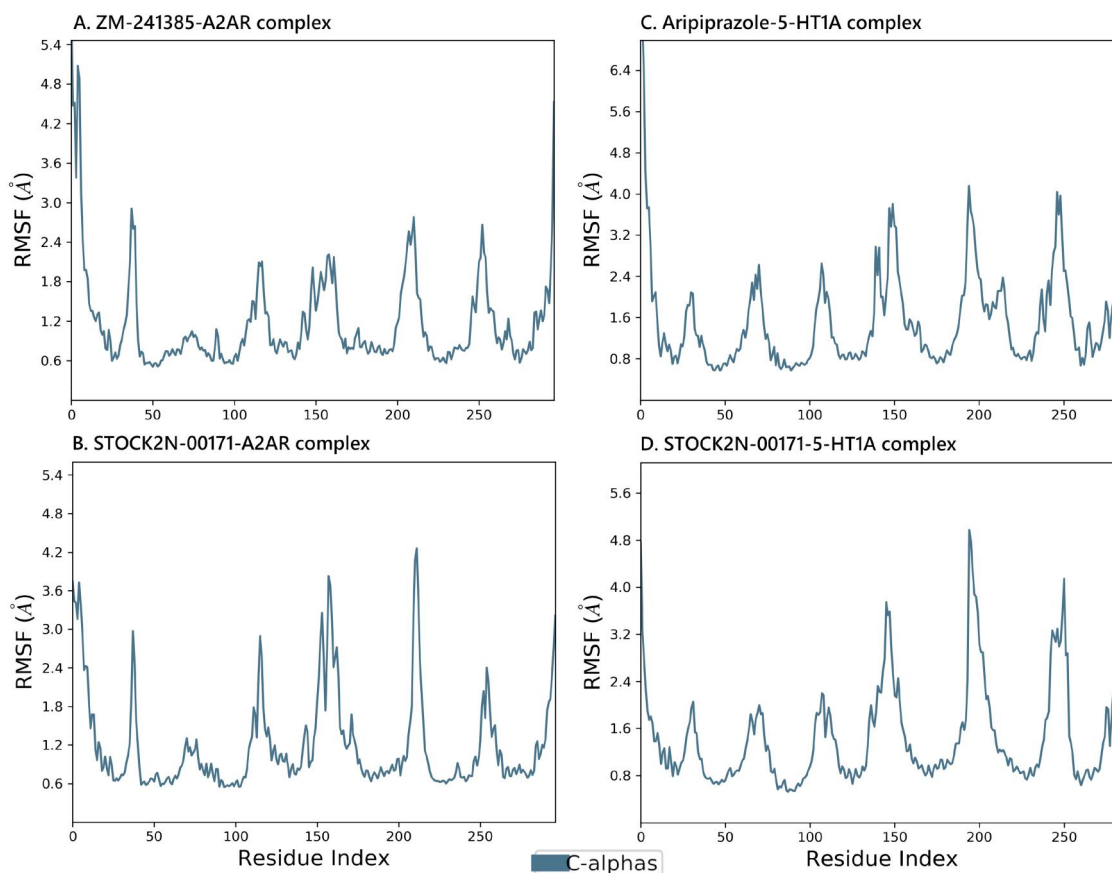


Figure 9. RMSF calculations of protein-ligand complexes throughout the 100 ns simulation time.

previously highlighted in the docking study, are stable and exhibit no fluctuations. These plots revealed that STOCK2N-00171-A2AR and STOCK2N-00171-5-HT1A complexes are stable throughout the simulation run.

3.5.3. Protein-ligand contact timeline

Figure 10 illustrates the timeline evolution of ligand-protein contacts (H-bonds, hydrophobic, ionic, and water bridges) during the 100 ns simulation period. The intensity of the band color positively correlates with the number of mediated contacts.

ZM-241385 totaled several nine interactions, with the maximum number of contacts being twelve. These interactions mainly involved Glu 169^{ECL2}, Leu 249^{6.51}, His 250^{6.52}, Asn 253^{6.55}, and Ala 273^{7.37}. These interactions differ in occupancy, with Glu 169^{ECL2} being the most consistent (as evident by the dark orange band). This is due to the different types of contacts mediated by this polar residue (hydrogen, water-mediated, and hydrophobic) as previously shown in Figure 6(A). Leu 249^{6.51} and Asn 253^{6.55} also displayed strong interactions which persisted throughout the production runtime. In the case of STOCK2N-00171, the ligand is averaging around five contacts, with the maximum being nine. Ile 80^{3.28}, Cys 166^{ECL2}, Phe 168^{ECL2}, and Asn 253^{6.55}, displayed consistent interactions with high to moderate occupancy. All contact with key amino acid residues was maintained throughout the simulation, except for Glu 169^{ECL2} which

formed transient interactions that persisted only for a fraction of the time.

Aripiprazole, in Figure 10(C), displayed on average six contacts, of which Asp 116^{3.32} made a stable and consistent interaction with the control. Tyr 96^{2.63} also established strong interactions with high occupancy. However, interactions involving Asn 100^{2.67}, Ile 113^{3.29}, Cys 120^{3.36}, Thr 188^{ECL2}, Ala 203^{5.46}, Trp 358^{6.48}, Phe 361^{6.51}, Met 377^{ECL3}, Thr 379^{7.31}, Asn 386^{7.38}, and Tyr 390^{7.42} were intermittent and inconsistent throughout the simulation. Whereas, STOCK2N-00171 established a high number of interactions with Asp 116, as indicated by the dark orange band in Figure 10(D). Although the ligand lost some interactions described earlier in the molecular docking study, several other residues have established contact, of which Tyr 96^{2.63}, Thr 188^{ECL2}, Ile 189^{ECL2}, Ser 374^{ECL3}, and Asn 386^{7.38} displayed the highest occupancy and persisted throughout the 100 ns simulation period.

3.5.4. Ligand property calculations

The stability of the selected complex was further examined using six parameters: Ligand RMSD, Radius of gyration (rGyr), Molecular surface area (MolSA), Solvent accessible surface area (SASA), and Polar surface area (PSA), results are shown in Figure 11.

The ligand RMSD for ZM-241385 exhibited some minor deviations in the first 40 ns and converged at around 1.4 Å for the rest of the simulation. The radius of gyration, which

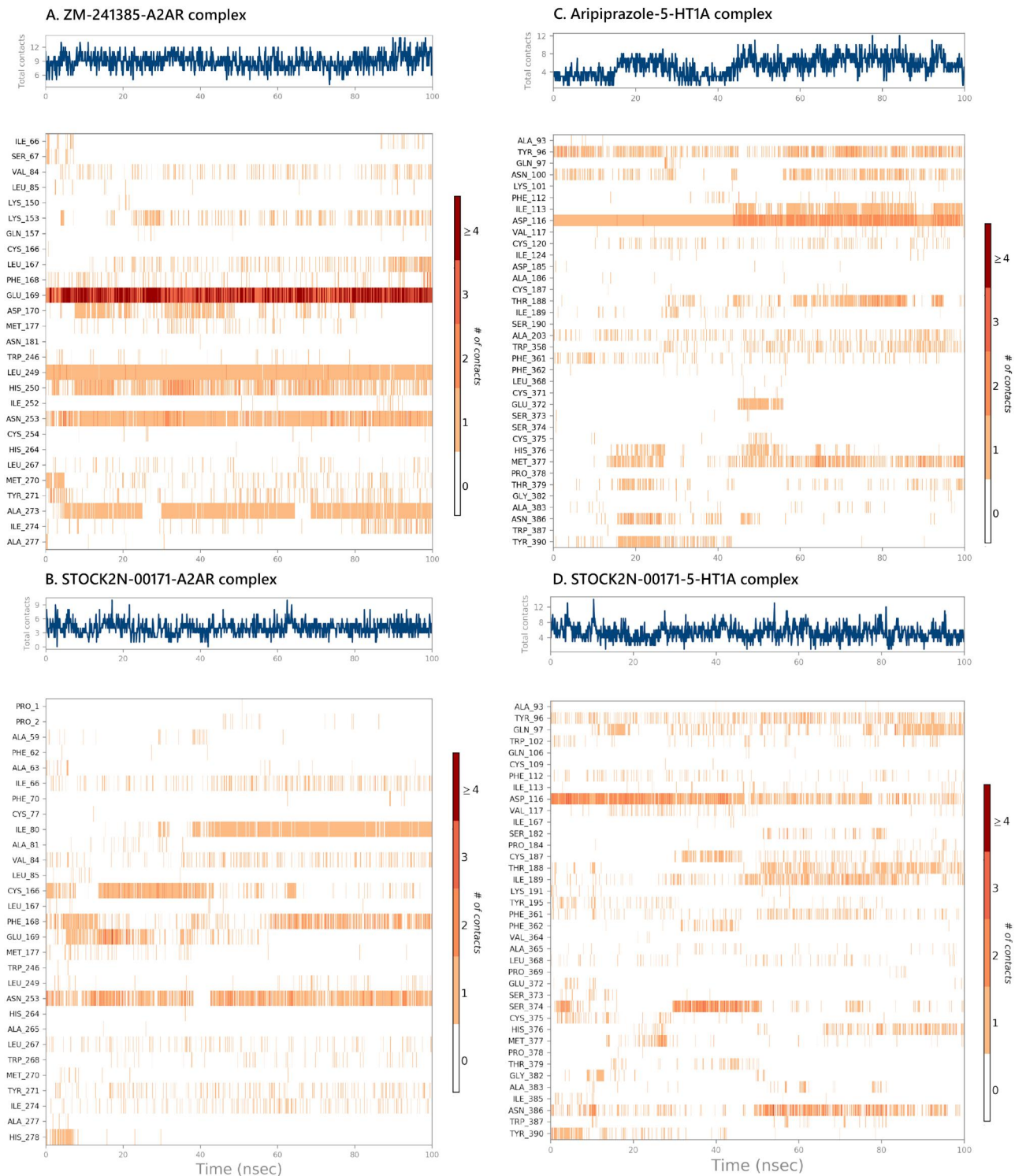


Figure 10. Timeline representation of ligand-protein contacts. The top panel represents the total number of contacts, while the heatmap shows the interacting amino acid residues.

describes the compactness of the ligand, reaches an equilibrium of $\approx 4.9\text{\AA}$ after the initial 50 ns, while MolSA remains constant throughout the simulation, averaging around 350\AA^2 . SASA fluctuates the most, with deviations reaching 120\AA^2 , gradually decreased and stabilized after the 70 ns mark and persisted at 60\AA^2 . The polar surface area was virtually stable at around 200\AA throughout the simulation, with slight deviations recorded at 30 and 75 ns. STOCK2N-00171 displayed a far more stable profile; ligand RMSD was stable

at 1.6\AA with practically no deviations after the initial 13 ns. The same observation can be made for rGyr, MolSA, SASA, and PSA, where the four reached equilibrium after the 40 ns mark and persisted at 5.3\AA , 480 , 125\AA^2 , and around 167\AA , respectively.

As for Aripiprazol, the ligand RMSD exhibited an upward trend, with spurts of fluctuations recorded at around 28 and 42 ns reaching 2.4 and 2 \AA , respectively. The plot stabilized at around 60 ns and persisted at 2.4\AA for the rest of the

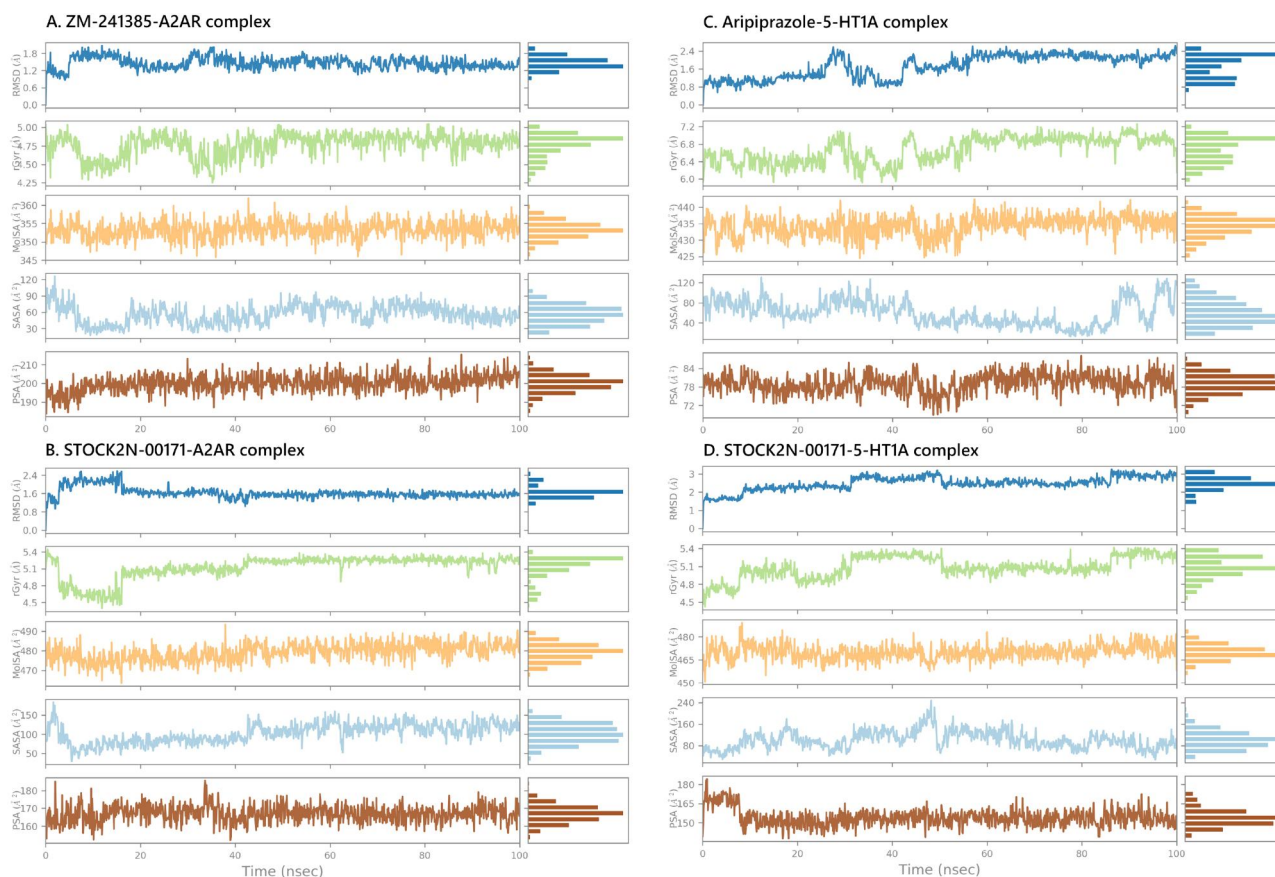


Figure 11. Ligand property calculations of the 4 protein-ligand complexes.

Table 6. MM-GBSA calculations.

| Complexes | ΔG_{Bind} | ΔG_{Coul} | ΔG_{Cov} | ΔG_{Hbond} | ΔG_{Lipo} | ΔG_{SolvGB} | ΔG_{Vdw} |
|----------------------|--------------------------|--------------------------|-------------------------|---------------------------|--------------------------|----------------------------|-------------------------|
| A2AR-ZM-241385 | -14.93 | 2.24 | 1.87 | -3.80 | -19.12 | 51.50 | -47.63 |
| 5-HT1A-Aripiprazole | -71.35 | -3.26 | 1.89 | -1.06 | -24.92 | 14.79 | -58.79 |
| A2AR-STOCK2N-00171 | -88.68 | -17.24 | 1.71 | -1.10 | -35.66 | 22.42 | -58.82 |
| 5-HT1A-STOCK2N-00171 | -65.60 | -1.34 | 4.24 | -0.09 | -26.71 | 21.43 | -63.11 |

ΔG_{Bind} : free energy of binding; ΔG_{Coul} : Coulomb energy; ΔG_{Cov} : covalent energy; ΔG_{Hbond} : hydrogen bonding energy; ΔG_{Lipo} : hydrophobic energy; ΔG_{SolvGB} : electrostatic solvation energy; ΔG_{Vdw} : Van der Waals energy.

simulation. rGyr showed a similar pattern, with equilibrium attained only after 60 ns, after which the values remained consistent at around 7 \AA^2 . MolSA had an overall stable profile at 433 \AA^2 followed by a dip after the initial 40 ns from then on the plot rose gradually and stabilized at 436 \AA^2 . SASA was somewhat consistent in the first 40 ns then gradually decreased reaching almost 0 \AA^2 around 80 ns only to start fluctuating by the end of the simulation reaching 120 \AA^2 . PSA was fairly stable throughout the simulation, with minor deviations spotted around 50 ns.

STOCK2N-00171 again exhibited a far more stable behavior with respect to the positive control, ligand RMSD showed very subtle fluctuations; the plot was stable at 2 \AA in the first 10–30 ns window, then it gradually rose to 3 \AA for a brief moment only to plateau at 2.5 \AA . The plot equilibrated at 3 \AA for the rest of the simulation. rGyr exhibited a similar profile, stabilizing at 5.3 \AA^2 after 90 ns. MolSA showed no visible fluctuations and persisted at around 470 \AA^2 for the whole simulation. SASA deviated in the initial 50 ns reaching 240 \AA^2 , only to plateau out at 80 \AA^2 near the end of the simulation.

PSA remained constant after the 7 ns mark and stabilized at around 150 \AA^2 for the rest of the simulation. The data presented here clearly indicates that the selected ligand was stable within the active site of the receptors.

3.5.5. MM-GBSA

Table 6 summarizes the binding free energy calculations for STOCK2N-00171, along with the two positive controls. The decomposition of the binding free energy revealed that van der Waals interactions along with lipophilicity and Coulomb's electrostatic attraction forces contributed significantly to the binding of STOCK2N-00171 to A2AR. The lead showed a low binding free energy (-88.68 Kcal/mol) in comparison to the control (-14.93 Kcal/mol), this is due to the cumulative effects of ΔG_{Coul} (-17.24 Kcal/mol), ΔG_{Lipo} (-35.66 Kcal/mol), and ΔG_{Vdw} (-58.82 Kcal/mol), where in the case of A2AR-ZM-241385, the Coulomb (2.24 Kcal/mol) and polar solvation energy (51.50 Kcal/mol) had unfavorable effects on the resulting binding energy, compromising, as a result, the affinity of

the control. By dissecting the total binding free energy for 5-HT1A complexes, it seems that Aripiprazole and STOCK2N-00171 had a similar profile with a ΔG_{Bind} of -71.35 and -65.60 Kcal/mol, respectively, with ΔG_{vdw} (-63.11 Kcal/mol) and ΔG_{Lipo} (-26.71 Kcal/mol) being the most favorable for the binding of the ligand. The low binding energies of STOCK2N-00171 are indicative of a stable interaction profile inside the binding pocket of A2AR and 5-HT1A.

The ligand-based pharmacophore modelling approach used in this study was successful in mapping potential active ligands against A2AR and 5-HT1A. The two selected models proved to be highly specific and sensitive, and were used to screen out the IBScreen natural database. Data from our results all point out that STOCK2N-00171 could be a promising scaffold for developing dual-acting ligands targeting A2A and 5-HT1A receptors. Post-MD analysis revealed that the ligand formed considerably stable complexes with both receptors, although some interactions reported in the molecular docking study were lost, the ligand is tightly bound to the binding cavities by strong and consistent interactions that persisted throughout the simulation runtime. Minor lapses seen in solubility can be corrected by further optimizing the ligand.

Some limitations that are worth flagging are the lack of experimental validation, however, based on the data of our computational analysis, we believe that the findings reported herein can serve as a molecular blueprint for the design and development of novel dual-acting ligands targeting A2A and 5-HT1A receptors for the treatment of Parkinson's disease.

4. Conclusion

Recent lines of evidence have pointed to the suppressing effect of combining A2AR antagonist with 5-HT1A agonist on involuntary movements induced by chronic use of Levodopa, unveiling as a result new and promising lines of treatment for Parkinson's disease.

Herein, we describe the identification of potential dual-acting ligands targeting A2A and 5-HT1A receptors, by means of ligand-based pharmacophore modelling, virtual screening, and molecular dynamics simulations. The constructed pharmacophore models proved to be highly sensitive and specific and accurately mapped potential actives from IBScreen database. The identified hit, STOCK2N-00171, had a low binding affinity with respect to drugs of reference, formed stable complexes throughout the simulation runtime, and had a favorable ADME profile.

On these bases, STOCK2N-00171 provides a molecular blueprint for the design of novel therapeutics targeting A2AR and 5-HT1A for Parkinson's disease therapy. Findings reported in this study warrant further experimental investigation to validate these results.

Notes

1. Evaluation of *Cardiospermum halicacabum* leaf compounds against human dihydroorotate dehydrogenase: A target for rheumatoid arthritis using structure based drug designing.
2. The PyMOL Molecular Graphics System, Version 2.0 Schrödinger, LLC.

Disclosure statement

No potential conflict of interest was reported by the author(s).

Funding

This work was supported by Princess Nourah bint Abdulrahman University Researchers Supporting Project number (PNURSP2023R437), Princess Nourah bint Abdulrahman University, Riyadh, Saudi Arabia. The authors received no financial support for the research, authorship, and/or publication of this article.

ORCID

Amal Maurady  <http://orcid.org/0000-0001-9298-717X>

References

- Abdalla, M., & Rabie, A. M. (2023). Dual computational and biological assessment of some promising nucleoside analogs against the COVID-19-omicron variant. *Computational Biology and Chemistry*, 104, 107768. <https://doi.org/10.1016/j.compbiolchem.2022.107768>
- Abdalla, M., Eltayb, W. A., El-Arabey, A. A., Singh, K., & Jiang, X. (2022). Molecular dynamic study of SARS-CoV-2 with various S protein mutations and their effect on thermodynamic properties. *Computers in Biology and Medicine*, 141, 105025. <https://doi.org/10.1016/j.compbiomed.2021.105025>
- Abdalla, M., Mohapatra, R. K., Sarangi, A. K., Mohapatra, P. K., Eltayb, W. A., Alam, M., El-Arabey, A. A., Azam, M., Al-Resayes, S. I., Seidel, V., & Dhama, K. (2021). *In silico* studies on phytochemicals to combat the emerging COVID-19 infection. *Journal of Saudi Chemical Society*, 25(12), 101367. <https://doi.org/10.1016/j.jscs.2021.101367>
- Azam, S., Haque, M. E., Jakaria, M., Jo, S. H., Kim, I. S., & Choi, D. K. (2020). G-protein-coupled receptors in CNS: A potential therapeutic target for intervention in neurodegenerative disorders and associated cognitive deficits. *Cells*, 9(2), 506. <https://doi.org/10.3390/cells9020506>
- Ballesteros, J. A., & Weinstein, H. (1995). [19] Integrated methods for the construction of three-dimensional models and computational probing of structure-function relations in G protein-coupled receptors. In *Methods in neurosciences* (Vol. 25, pp. 366–428). Academic Press.
- Berman, H., Henrick, K., & Nakamura, H. (2003). Announcing the worldwide protein data bank. *Nature Structural Biology*, 10(12), 980–980. <https://doi.org/10.1038/nsb1203-980>
- Bowers, K. J., Chow, E., Xu, H., Dror, R. O., Eastwood, M. P., Gregersen, B. A., Klepeis, J. L., Kolossvary, I., Moraes, M. A., Sacerdoti, F. D., Salmon, J. K., Shan, Y., Shaw, D. E. (2006, November). Scalable algorithms for molecular dynamics simulations on commodity clusters. In *Proceedings of the 2006 ACM/IEEE Conference on Supercomputing* (p. 84-es). <https://doi.org/10.1145/1188455.1188544>
- Cenci, M. A., Skovgård, K., & Odin, P. (2022). Non-dopaminergic approaches to the treatment of motor complications in Parkinson's disease. *Neuropharmacology*, 210, 109027. <https://doi.org/10.1016/j.neuropharm.2022.109027>
- Chen, J. F., & Cunha, R. A. (2020). The belated US FDA approval of the adenosine A_{2A} receptor antagonist istradefylline for treatment of Parkinson's disease. *Purinergic Signalling*, 16(2), 167–174. <https://doi.org/10.1007/s11302-020-09694-2>
- Cieślak, M., Komoszyński, M., & Wojtczak, A. (2008). Adenosine A_{2A} receptors in Parkinson's disease treatment. *Purinergic Signalling*, 4(4), 305–312. <https://doi.org/10.1007/s11302-008-9100-8>
- Cotzias, G. C., Papavasiliou, P. S., & Gellene, R. (1969). Modification of Parkinsonism—Chronic treatment with L-dopa. *The New England Journal of Medicine*, 280(7), 337–345. <https://doi.org/10.1056/NEJM196902132800701>
- Dixon, S. L., Smondryev, A. M., & Rao, S. N. (2006). PHASE: A novel approach to pharmacophore modeling and 3D database searching. *Chemical Biology & Drug Design*, 67(5), 370–372. <https://doi.org/10.1111/j.1747-0285.2006.00384.x>

- Dixon, S. L., Smondyrev, A. M., Knoll, E. H., Rao, S. N., Shaw, D. E., & Friesner, R. A. (2006). PHASE: A new engine for pharmacophore perception, 3D QSAR model development, and 3D database screening. 1. Methodology and preliminary results. *Journal of Computer-Aided Molecular Design*, 20(10–11), 647–671. <https://doi.org/10.1007/s10822-006-9087-6>
- Dupre, K. B., Eskow, K. L., Steiniger, A., Klioueva, A., Negron, G. E., Lormand, L., Park, J. Y., & Bishop, C. (2008). Effects of coincident 5-HT_{1a} receptor stimulation and NMDA receptor antagonism on L-DOPA-induced dyskinesia and rotational behaviors in the hemi-parkinsonian rat. *Psychopharmacology*, 199(1), 99–108. <https://doi.org/10.1007/s00213-008-1135-6>
- Eltayb, W. A., Abdalla, M., & Rabie, A. M. (2023). Novel Investigational Anti-SARS-CoV-2 Agent Ensitrelvir “S-217622”: A very promising potential universal broad-spectrum antiviral at the therapeutic front-line of coronavirus species. *ACS Omega*, 8(6), 5234–5246. <https://doi.org/10.1021/acsomega.2c03881>
- Eltayb, W. A., Abdalla, M., El-Arabey, A. A., Boufissiou, A., Azam, M., Al-Resayes, S. I., & Alam, M. (2023). Exploring particulate methane monooxygenase (pMMO) proteins using experimentation and computational molecular docking. *Journal of King Saud University-Science*, 35(4), 102634. <https://doi.org/10.1016/j.jksus.2023.102634>
- Friesner, R. A., Banks, J. L., Murphy, R. B., Halgren, T. A., Klicic, J. J., Mainz, D. T., Repasky, M. P., Knoll, E. H., Shelley, M., Perry, J. K., Shaw, D. E., Francis, P., & Shenkin, P. S. (2004). Glide: A new approach for rapid, accurate docking and scoring. 1. Method and assessment of docking accuracy. *Journal of Medicinal Chemistry*, 47(7), 1739–1749. <https://doi.org/10.1021/jm0306430>
- Friesner, R. A., Murphy, R. B., Repasky, M. P., Frye, L. L., Greenwood, J. R., Halgren, T. A., Sanschagrin, P. C., & Mainz, D. T. (2006). Extra precision glide: Docking and scoring incorporating a model of hydrophobic enclosure for protein-ligand complexes. *Journal of Medicinal Chemistry*, 49(21), 6177–6196. <https://doi.org/10.1021/jm0512560>
- Gaulton, A., Bellis, L. J., Bento, A. P., Chambers, J., Davies, M., Hersey, A., Light, Y., McGlinchey, S., Michalovich, D., Al-Lazikani, B., & Overington, J. P. (2012). ChEMBL: A large-scale bioactivity database for drug discovery. *Nucleic Acids Research*, 40(Database issue), D1100–D1107. <https://doi.org/10.1093/nar/gkr777>
- Ghiglieri, V., Mineo, D., Vannelli, A., Cacace, F., Mancini, M., Pendolino, V., Napolitano, F., di Maio, A., Mellone, M., Stanic, J., Tronci, E., Fidalgo, C., Stancampiano, R., Carta, M., Calabresi, P., Gardoni, F., Usiello, A., & Picconi, B. (2016). Modulation of serotonergic transmission by eltopazine in L-DOPA-induced dyskinesia: Behavioral, molecular, and synaptic mechanisms. *Neurobiology of Disease*, 86, 140–153. <https://doi.org/10.1016/j.nbd.2015.11.022>
- Giordano, D., Biancaniello, C., Argenio, M. A., & Facchiano, A. (2022). Drug design by pharmacophore and virtual screening approach. *Pharmaceuticals*, 15(5), 646. <https://doi.org/10.3390/ph15050646>
- Glass, M., Faull, R. L. M., & Dragunow, M. (1996). Localisation of the adenosine uptake site in the human brain: A comparison with the distribution of adenosine A₁ receptors. *Brain Research*, 710(1–2), 79–91. [https://doi.org/10.1016/0006-8993\(95\)01318-0](https://doi.org/10.1016/0006-8993(95)01318-0)
- Hadni, H., & Elhallaouia, M. (2022). *In silico* design of EGFR^{L858R/T790M}/C797S inhibitors via 3D-QSAR, molecular docking, ADMET properties and molecular dynamics simulations. *Heliyon*, 8(11), e11537. <https://doi.org/10.1016/j.heliyon.2022.e11537>
- Hauser, A. S., Attwood, M. M., Rask-Andersen, M., Schiöth, H. B., & Gloriam, D. E. (2017). Trends in GPCR drug discovery: New agents, targets and indications. *Nature Reviews. Drug Discovery*, 16(12), 829–842. <https://doi.org/10.1038/nrd.2017.178>
- Hilger, D., Masureel, M., & Kobilka, B. K. (2018). Structure and dynamics of GPCR signaling complexes. *Nature Structural & Molecular Biology*, 25(1), 4–12. <https://doi.org/10.1038/s41594-017-0011-7>
- Huang, N., Shoichet, B. K., & Irwin, J. J. (2006). Benchmarking sets for molecular docking. *Journal of Medicinal Chemistry*, 49(23), 6789–6801. <https://doi.org/10.1021/jm0608356>
- Jacobson, M. P., Friesner, R. A., Xiang, Z., & Honig, B. (2002). On the role of the crystal environment in determining protein side-chain conformations. *Journal of Molecular Biology*, 320(3), 597–608. [https://doi.org/10.1016/S0022-2836\(02\)00470-9](https://doi.org/10.1016/S0022-2836(02)00470-9)
- Jacobson, M. P., Pincus, D. L., Rapp, C. S., Day, T. J., Honig, B., Shaw, D. E., & Friesner, R. A. (2004). A hierarchical approach to all-atom protein loop prediction. *Proteins*, 55(2), 351–367. <https://doi.org/10.1002/prot.10613>
- Jarvis, M. F., Jackson, R. H., & Williams, M. (1989). Autoradiographic characterization of high-affinity adenosine A₂ receptors in the rat brain. *Brain Research*, 484(1–2), 111–118. [https://doi.org/10.1016/0006-8993\(89\)90353-3](https://doi.org/10.1016/0006-8993(89)90353-3)
- Kim, S., Chen, J., Cheng, T., Gindulyte, A., He, J., He, S., Li, Q., Shoemaker, B. A., Thiessen, P. A., Yu, B., Zaslavsky, L., Zhang, J., & Bolton, E. E. (2019). PubChem 2019 update: Improved access to chemical data. *Nucleic Acids Research*, 47(D1), D1102–D1109. <https://doi.org/10.1093/nar/gky1033>
- King, M. V., Marsden, C. A., & Fone, K. C. (2008). A role for the 5-HT_{1A}, 5-HT₄ and 5-HT₆ receptors in learning and memory. *Trends in Pharmacological Sciences*, 29(9), 482–492. <https://doi.org/10.1016/j.tips.2008.07.001>
- Kroeze, W. K., Kristiansen, K., & Roth, B. L. (2002). Molecular biology of serotonin receptors-structure and function at the molecular level. *Current Topics in Medicinal Chemistry*, 2(6), 507–528. <https://doi.org/10.2174/1568026023393796>
- Kumar, A., Agarwal, P., Rathi, E., & Kini, S. G. (2022). Computer-aided identification of human carbonic anhydrase isoenzyme VII inhibitors as potential antiepileptic agents. *Journal of Biomolecular Structure & Dynamics*, 40(11), 4850–4865. <https://doi.org/10.1080/07391102.2020.1862706>
- Lane, J. R., Herenbrink, C. K., Van Westen, G. J., Spoorendonk, J. A., Hoffmann, C., & Ilzerman, A. P. (2012). A novel nonribose agonist, LUF5834, engages residues that are distinct from those of adenosine-like ligands to activate the adenosine A_{2A} receptor. *Molecular Pharmacology*, 81(3), 475–487. <https://doi.org/10.1124/mol.111.075937>
- Lebon, G., Warne, T., Edwards, P. C., Bennett, K., Langmead, C. J., Leslie, A. G., & Tate, C. G. (2011). Agonist-bound adenosine A_{2A} receptor structures reveal common features of GPCR activation. *Nature*, 474(7352), 521–525. <https://doi.org/10.1038/nature10136>
- LigPrep (2021). *Schrödinger Release 2022-3: LigPrep*. Schrödinger, LLC.
- Liu, Y., Sun, C., Hao, Y., Jiang, T., Zheng, L., & Wang, S. (2010). Mechanism of dissolution enhancement and bioavailability of poorly water soluble celecoxib by preparing stable amorphous nanoparticles. *Journal of Pharmacy & Pharmaceutical Sciences*, 13(4), 589–606. <https://doi.org/10.18433/j3530j>
- Lütjens, R., & Rocher, J. P. (2017). Recent advances in drug discovery of GPCR allosteric modulators for neurodegenerative disorders. *Current Opinion in Pharmacology*, 32, 91–95. <https://doi.org/10.1016/j.coph.2017.01.001>
- Madhavi Sastry, G., Adzhigirey, M., Day, T., Annabhimoju, R., & Sherman, W. (2013). Protein and ligand preparation: Parameters, protocols, and influence on virtual screening enrichments. *Journal of Computer-Aided Molecular Design*, 27(3), 221–234. <https://doi.org/10.1007/s10822-013-9644-8>
- Mori, A. (2020). How do adenosine A_{2A} receptors regulate motor function? *Parkinsonism & Related Disorders*, 80 Suppl 1, S13–S20. <https://doi.org/10.1016/j.parkreldis.2020.09.025>
- Mori, A., Chen, J. F., Uchida, S., Durlach, C., King, S. M., & Jenner, P. (2022). The pharmacological potential of adenosine A_{2A} receptor antagonists for treating Parkinson’s disease. *Molecules*, 27(7), 2366. <https://doi.org/10.3390/molecules27072366>
- Moussa, N., Hassan, A., & Gharaghani, S. (2021). Pharmacophore model, docking, QSAR, and molecular dynamics simulation studies of substituted cyclic imides and herbal medicines as COX-2 inhibitors. *Heliyon*, 7(4), e06605. <https://doi.org/10.1016/j.heliyon.2021.e06605>
- Munk, C., Isberg, V., Mordalski, S., Harpsøe, K., Rataj, K., Hauser, A. S., Kolb, P., Bojarski, A. J., Vriend, G., & Gloriam, D. E. (2016). GPCRdb: The G protein-coupled receptor database—An introduction. *British Journal of Pharmacology*, 173(14), 2195–2207. <https://doi.org/10.1111/bph.13509>
- Novikov, G. V., Sivozhelezov, V. S., & Shaitan, K. V. (2013). Investigation of the conformational dynamics of the A_{2A} adenosine receptor by molecular dynamics simulation. *Biophysics*, 58(4), 482–492. <https://doi.org/10.1134/S0006350913040131>

- Ohno, Y., Shimizu, S., Tokudome, K., Kunisawa, N., & Sasa, M. (2015). New insight into the therapeutic role of the serotonergic system in Parkinson's disease. *Progress in Neurobiology*, 134, 104–121. <https://doi.org/10.1016/j.pneurobio.2015.09.005>
- Pinna, A., Parekh, P., & Morelli, M. (2023). Serotonin 5-HT1A receptors and their interactions with adenosine A2A receptors in Parkinson's disease and dyskinesia. *Neuropharmacology*, 226, 109411. <https://doi.org/10.1016/j.neuropharm.2023.109411>
- Politis, M., Wu, K., Loane, C., Brooks, D. J., Kiferle, L., Turkheimer, F. E., Bain, P., Molloy, S., & Piccini, P. (2014). Serotonergic mechanisms responsible for levodopa-induced dyskinesias in Parkinson's disease patients. *The Journal of Clinical Investigation*, 124(3), 1340–1349. <https://doi.org/10.1172/JCI71640>
- Rahman, M. M., Islam, M. R., Mim, S. A., Sultana, N., Chellappan, D. K., Dua, K., Kamal, M. A., Sharma, R., & Emran, T. B. (2022). Insights into the promising prospect of G protein and GPCR-mediated signaling in neuropathophysiology and its therapeutic regulation. *Oxidative Medicine and Cellular Longevity*, 2022, 8425640. <https://doi.org/10.1155/2022/8425640>
- Rascol, O., Brooks, D. J., Melamed, E., Oertel, W., Poewe, W., Stocchi, F., & Tolosa, E. (2005). Rasagiline as an adjunct to levodopa in patients with Parkinson's disease and motor fluctuations (LARGO, Lasting effect in Adjunct therapy with Rasagiline given once daily, study): A randomised, double-blind, parallel-group trial. *Lancet*, 365(9463), 947–954. [https://doi.org/10.1016/S0140-6736\(05\)71083-7](https://doi.org/10.1016/S0140-6736(05)71083-7)
- Schiffmann, S. N., Fisone, G., Moresco, R., Cunha, R. A., & Ferré, S. (2007). Adenosine A2A receptors and basal ganglia physiology. *Progress in Neurobiology*, 83(5), 277–292. <https://doi.org/10.1016/j.pneurobio.2007.05.001>
- Schrödinger, LLC (2021a). *Schrödinger Release 2023-1: Protein Preparation Wizard*. Epik, Schrödinger, LLC; Impact, Schrödinger, LLC; Prime, Schrödinger, LLC.
- Schrödinger, LLC (2021b). *Schrödinger Release 2023-1: QikProp*. Author.
- Schrödinger, LLC (2021c). *Schrödinger Release 2023-1: Desmond molecular dynamics system*. D. E. Shaw Research; Maestro-Desmond Interoperability Tools, Schrödinger.
- Schrödinger, LLC (2021d). *Schrödinger Release 2023-1: Prime*. Author.
- Sukalovic, V., Ignjatovic, D., Tovilovic, G., Andric, D., Shakib, K., Kostic-Rajacic, S., & Soskic, V. (2012). Interactions of *N*-{[2-(4-phenylpiperazin-1-yl)-ethyl]-phenyl}-2-aryl-2-yl-acetamides and 1-{[2-(4-phenylpiperazin-1-yl)-ethyl]-phenyl}-3-aryl-2-yl-ureas with dopamine D2 and 5-hydroxytryptamine 5HT1A receptors. *Bioorganic & Medicinal Chemistry Letters*, 22(12), 3967–3972. <https://doi.org/10.1016/j.bmcl.2012.04.098>
- Sveinbjornsdottir, S. (2016). The clinical symptoms of Parkinson's disease. *Journal of Neurochemistry*, 139 Suppl 1(S1), 318–324. <https://doi.org/10.1111/jnc.13691>
- Tolosa, E., Martí, M. J., Valldeoriola, F., & Molinuevo, J. L. (1998). History of levodopa and dopamine agonists in Parkinson's disease treatment. *Neurology*, 50(6 Suppl 6), S2–S10. https://doi.org/10.1212/wnl.50.6_suppl_6.s2
- Xiong, G., Wu, Z., Yi, J., Fu, L., Yang, Z., Hsieh, C., Yin, M., Zeng, X., Wu, C., Lu, A., Chen, X., Hou, T., & Cao, D. (2021). ADMETlab 2.0: An integrated online platform for accurate and comprehensive predictions of ADMET properties. *Nucleic Acids Research*, 49(W1), W5–W14. <https://doi.org/10.1093/nar/gkab255>
- Xu, K., Bastia, E., & Schwarzschild, M. (2005). Therapeutic potential of adenosine A2A receptor antagonists in Parkinson's disease. *Pharmacology & Therapeutics*, 105(3), 267–310. <https://doi.org/10.1016/j.pharmthera.2004.10.007>
- Zlatović, M. V., Šukalović, V. V., Schneider, C., & Roglić, G. M. (2006). Interaction of arylpiperazine ligands with the hydrophobic part of the 5-HT1A receptor binding site. *Bioorganic & Medicinal Chemistry*, 14(9), 2994–3001. <https://doi.org/10.1016/j.bmc.2005.12.023>